Journal of Materials Chemistry A

Accepted Manuscript

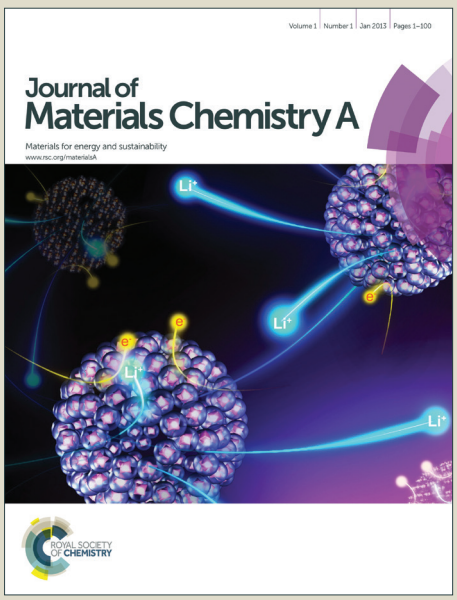

ROYAL SOCIETY OF CHEMISTRY

www.rsc.org/materialsA

Unique Synthesis of Novel Octahedral Micro/Nano Hierarchical $LiFePO_4$ Cages as an Enhanced Cathode Material for Lithium-ion Batteries

*Wenxiang Li, Huijuan Zhang, Yanping Mu, Li Liu, Yu Wang**

The State Key Laboratory of Mechanical Transmissions and the School of Chemistry and Chemical Engineering, Chongqing University, 174 Shazheng Street, Shapingba District, Chongqing City, P.R. China, 400044.

E-mail: wangy@cqu.edu.cn; prospectwy@gmail.com

Keywords: Octahedral, Micro/nano, $LiFePO_4$, Cathode material, Lithium-ion batteries

Abstract: Novel Monodispersed $LiFePO_4$ cages with octahedral micro/nano hierarchical structure, have been firstly synthesized through a simple and controllable solvothermal approach followed by high-temperature calcinations. The structural characterizations are investigated using X-ray diffraction, scanning electron microscope, Brunauer-Emmett-Teller surface area measurements, Raman spectroscopy and X-ray energy dispersive spectroscopy. As detected, our unique octahedral micro/nano $LiFePO_4$ cages possess numerous outstanding properties, such as single-crystalline, hierarchical structure and large specific surface areas, which significantly lends to high rate capability, excellent cycling stability and superior tap density. This special micro/nano hierarchical structure can be extended to other lithium metal oxide composites, which would promote the development of lithium-ion batteries.

Introduction

As excellent reversible electrochemical energy storage (EES) devices, rechargeable lithium-ion batteries (LIBs) are evidenced to be the predominant power sources for electric vehicles (EVs) and hybrid electric vehicles (HEVs), owning to their long cycle life, high energy density and capacity.[1-3] As for the major building blocks of LIBs, cathode materials are still believed one of the greatest challenges on the electrochemical performance and practical applications.[4, 5] Among the families of cathode materials, the olivine-type lithium iron(II) phosphate ($LiFePO_4$), proposed by Padhi et al.,[6] is now considered as the most promising candidate for next generation of green and sustainable lithium-ion battery system due primarily to its high operating voltage (~3.4V vs Li/Li^+), large theoretical capacity (~170 mAh g^{-1}), abundant resources, environmental friendliness and thermal stability.[7-9] However, even with these chief advantages, the capacity and rate performance of $LiFePO_4$ are seriously limited by the low inherent electronic conductivity and the sluggish diffusion of lithium ions,[10] which hinder its large-scale applications.[11] In the last decades, various strategies have been tried to overcome the intrinsic problems of $LiFePO_4$.[12-15] Among these methods, doping with foreign atoms and coating with electronically conductive agents have been demonstrated to be efficacious approaches to improve the electronic conductivity. And decreasing the size of $LiFePO_4$ particles to nanoscale will enhance the high-rate performance by shortening the Li^+ diffusion distance and increasing the effective reaction areas.

According to the diffusion equation $t=L^2/2D$ (where t is the diffusion time, L is the diffusion distance, and D is the diffusion coefficient),[16] the Li^+ diffusion time depends on diffusion distance. As a result, decreasing the size to nanoscale can facilitate Li^+ transfer to improve the rate capability.[17, 18] And nanoscale materials, especially with designed structure, have attracted extensive interests because of their high-rate performance and high specific surface areas.[19-21] Nevertheless, nanoscale $LiFePO_4$ materials still face its obstacles for practical applications: (a) $LiFePO_4$ nanoparticles easily occur agglomeration because of their high interfacial energy, which severely affect voltage plateau and cycling stability;[22] (b) nanoscale $LiFePO_4$ particles will fall off the current collector (aluminum foil) easily, which need more polymeric binder than that of micro-sized particles, thereby resulting in the decrease

of tap density.[23, 24] Therefore, the tap density is sacrificed when nanoscale materials achieved high rate capability. Furthermore, the low tap density seriously limits the volumetric power density of a lithium-ion battery. As a contrast, the tap density of $LiFePO_4$ nanopaticles and irregular carbon coating is generally less than 1.0 g cm^{-3}.[25] However, micro-sized $LiFePO_4$/C composites own a high tap density.[23, 26] (even 1.6 g cm^{-3} [27]) (c) $LiFePO_4$ nanoparticles can increase the surface area and at the same time manifold the adverse electrode/electrolyte reactions, leading to a worse cycling performance.[28] Thus, it is vital to project effective method to enhance the electrochemical properties and practical applications. Fabricating micro/nano hierarchical structure is a feasible approach because it can take the advantages of nanoparticles and micro-sized structure.[25, 29, 30] Primary $LiFePO_4$ nanoparticles will improve the high-rate performance by shortening Li^+ diffusion distance and increasing the effective reaction areas. And secondary micro-sized structure will assure high tap density and cycling stability.

Herein, by designing and controlling the morphology and structure of $LiFePO_4$, we have firstly synthesized monodispersed $LiFePO_4$ single-crystalline with octahedral micro/nano hierarchical structure using a controllable solvothermal approach and high-temperature calcination. This special micro/nano hierarchical structure gives rise to enhanced electrochemical performance. Secondary micro-sized octahedral structure composed of $LiFePO_4$ nanoparticles will assure high tap density and cycling stability. Primary $LiFePO_4$ nanoparticles will improve the high-rate performance. The interstices between primary $LiFePO_4$ nanoparticles are beneficial for electrolyte penetration, accelerating the insertion/extraction reaction. As expected, the as-prepared $LiFePO_4$ shows high-rate performance, long lifetime and excellent tap density as cathode for LIBs. In light of this observation, $LiFePO_4$ with octahedral micro/nano hierarchical structure can be a valid approach to surmount the inherent problems of $LiFePO_4$ for practical applications, which would promote the development of lithium-ion batteries.

Results and Discussions

The whole synthesis process of monodispersed octahedral micro/nano hierarchical $LiFePO_4$ cages is schematically illustrated in Figure 1. In the experiment, the precursor of $Fe_3(PO_4)_2(OH)_2$ with micro-sized octahedral structure morphology has been firstly synthesized by a solvothermal method. Thinking about the strong chelating ability,[31, 32] we adopt ethylene glycol as the solvent in the process. Na_2CO_3, which possesses a large amount of CO_3^{2-}, is usually employed as the precipitant to deposit the precursor.[33, 34] As proved by Shi in the previous report, the synthesized materials present smaller size and higher discharge capacity when adding Na_2CO_3 as the precipitant.[35] The formation mechanism of $Fe_3(PO_4)_2(OH)_2$ with octahedral structure seems to be similar with that of single-crystalline iron oxide nanotubes. In this process, phosphate ions are very important factor because of their different adsorption ability on the different crystal planes and the coordination effect with Fe^{3+}.[36] We propose that the adsorption capacities for phosphate to $Fe_3(PO_4)_2(OH)_2$ are much higher for (111) planes than for the others, and the coordination effect of phosphate ions with Fe^{3+} ions is another crucial aspect. As (111) planes of $Fe_3(PO_4)_2(OH)_2$ are given in the Figures S1 (Supporting Information), the absorbed phosphate ions cannot be removed easily and protect the precursor from further reaction. As a result, (111) crystal planes and the equivalent crystal planes become more stable and finally develop into tetragonal $Fe_3(PO_4)_2(OH)_2$. Subsequently, the solid-state reaction between the above tetragonal $Fe_3(PO_4)_2(OH)_2$ crystals and the lithium orthophosphate at the molar ratio of 1:1 are carried out at 700 ^oC in Ar atmosphere. According to chemical reaction equation $Fe_3(PO_4)_2(OH)_2 + Li_3PO_4 + C \rightarrow 3LiFePO_4 + CO + H_2O$, $LiFePO_4$ cages with octahedral micro/nano hierarchical structure can be achieved due to the release of CO and H_2O gas. The thermogravimetric analysis curve of $LiFePO_4$ is shown in Figure S4 (Supporting Information). From the TGA curve, we can see that the actual weight gain of the $LiFePO_4$ cages nearly equal to the theoretical weight gain (5.07%) proposed by M.S. Whittingham,[37] indicating the carbon used as reducing agent completely transformed.

The phase purity and structural characterization of the tetragonal $Fe_3(PO_4)_2(OH)_2$ crystals are shown in Figure 2.

The X-ray diffraction (XRD) pattern of the precursor in Figure 2a shows highly crystalline. All of the Bragg peaks can be clearly indexed to tetragonal $Fe_3(PO_4)_2(OH)_2$ phase (JCPDS No.45-1454). Figure 2b and 2c are the low-magnification scanning electron microscopy (SEM) images. It is observed that the precursor of tetragonal $Fe_3(PO_4)_2(OH)_2$ with uniform size of 6~7 μm diameter can be easily obtained in large scale after a solvothermal reaction for 24 hrs. Furthermore, high-resolution transmission electron microscopy (HRTEM) image (Figure 2d) also demonstrates the monocrystal nature. And its interplanar distance of ~0.315 nm corresponds to the (121) plane of $Fe_3(PO_4)_2(OH)_2$.

Afterwards, $LiFePO_4$ with the octahedral micro/nano hierarchical structure has been perfectly fabricated after thermal transformation. The phase purity and structural details of the micro/nano hierarchical structure are also characterized by XRD, SEM, HRTEM as shown in Figure 3 and Fourier transform infrared spectroscopy (FTIR) as shown in Figure S3 (Supporting Information), respectively. As the XRD patterns (Figure 3a) revealed, all the Bragg peaks ranging 5~90 degrees are in good agreement with orthorhombic $LiFePO_4$ phase (JCPDS No.81-1173). Commercial $LiFePO_4$ powders are utilized to be comparison on electrochemical capacity. From SEM image (Figure 3b), it can be observed that as-prepared $LiFePO_4$ cages are well dispersed and micro-sized particle size identically matches with the precursor. The enlarged SEM image in Figure 3c shows that single micro-sized octahedral structure possesses plenty of interstices, providing the sufficient interface between electrolyte and active materials, which is beneficial for enhancing electrochemical performances. Micro-sized octahedral structure is constructed by $LiFePO_4$ nanoparticles around 200~300 nm diameter as shown in the inset of Figure 3c, which not only effectively prevent nanoparticle from aggregation and present excellent cycling stability, but also improve the rate capability. Combining the HRTEM image in Figure 3d with the XRD data in Figure 3a, it is revealed that the obtained micro/nano hierarchical $LiFePO_4$ cages are pure–phase and single crystal, and the lattice spacing of ~0.226 nm can be assigned to the (401) plane of orthorhombic $LiFePO_4$ phase. FTIR spectrum (Figures S3 Supporting Information) is to examine the antisite defect.[38] The infrared absorption peak at about 950 cm^{-1} corresponds to symmetric stretching P-O peak in PO_4 tetrahedron, demonstrating the lower antisite defect concentration in octahedral micro/nano hierarchical structured $LiFePO_4$.

Nitrogen isothermal adsorption-desorption measurements are performed to determine the porous structure and Brunauer-Emmett-Teller (BET) surface areas of the $LiFePO_4$ cages. According to BET analysis in Figure 4, a total specific surface area of 40.631 $m^2 g^{-1}$ is obtained. The Barrett-Joyner-Halenda (BJH) pore-size distribution, shown in the inset of Figure 4, indicates that the pore size mainly focused at 31.2 nm and 53.7 nm, respectively. The large surface area will be beneficial for providing a sufficient interface between electrolyte and electrode materials.

The cathode electrochemical characterizations of the monodispersed $LiFePO_4$ cages with octahedral micro/nano hierarchical structure are shown in Figure 5. Figure 5a shows the first two cyclic voltammograms (CV) of the micro/nano hierarchical $LiFePO_4$ cages in the voltage window of 2.4 ~ 4.2 V at a scan rate of 0.5 mV s^{-1}, which CV behavior is generally consistent with those of $LiFePO_4$ materials reported in the literature.[39] It can be seen that two well-defined redox peaks are observed between 3.3 V and 3.6 V, corresponding to the Li^+ insertion/extraction in $LiFePO_4$. The galvanostatic discharge and charge curves of as-prepared $LiFePO_4$ electrode ranging from 2.0 ~ 4.2 V at a current density of 17 mA g^{-1} (0.1 C) are presented in Figure 5b. The discharge and charge specific capacities are 140 and 146 mAh g^{-1}, respectively, showing Coulombic efficiency of 96% for the initial cycle. The specific capacity is almost similar to those of porous $LiFePO_4$ microspheres[25], mesoporous $LiFePO_4$/C nanocomposites[40] and $LiFePO_4$ nanoparticles encapsulated in graphene nanoshells[39]. The shape of curves almost has no change during 500th cycling with capacity retention of 98%, demonstrating the excellent stability of micro-sized octahedral cages. As observed the SEM images in Figure S2 (Supporting Information), the structural sturdiness of micro/nano hierarchical $LiFePO_4$ cages is well retained. Figure 5c shows the rate performance of the micro/nano hierarchical $LiFePO_4$ cages electrode (black dot) and commercial $LiFePO_4$/C powders electrode (red

dot). It is observed that both capacity decreases with the increase of current densities. The micro/nano hierarchical $LiFePO_4$ cages electrode discloses more stable discharge plateau than that of commercial $LiFePO_4$/C powders electrode as the C-rate increasing. The as-prepared $LiFePO_4$ presents discharge capacity of 106, 88 and 76 mAh g^{-1} at the C-rate of 5, 10 and 20, respectively. Commercial $LiFePO_4$/C just deliver 82, 56 and 43 mAh g^{-1} at the corresponding C-rates. In comparison, the rate capacity is also higher than $LiFePO_4$ materials[41] and solid $LiFePO_4$ microspheres[42], which can be associated with diffusion distance shortening by nanoscale particles and well-crystallized nanoparticles. Cycling stability of the as-prepared $LiFePO_4$ during long-term discharge/charge cycles at a current density of 1700 mA g^{-1} (10 C) is shown in Figure 5d. The discharge capacity of sample can remain at 85 mAh g^{-1}, which is also higher than those of previous reports,[43, 44] indicating the good rate capability of micro/nano $LiFePO_4$ cages. The Coulombic efficiency of as-prepared $LiFePO_4$ electrode approaches ~100% over the first few cycles, signifying its excellent reversibility.

Noteworthily, morphology and crystallinity of as-prepared $LiFePO_4$ are well maintained. Furthermore, the temperature-dependent electrochemical performances are measured with the testing temperature 0, 25 and 50 ^oC (Figure S5, Supporting Information). As expected, the discharge capacity gradually increases with the testing temperature varying from 0, to 25 and 50 ^oC. Moreover, the electrochemical impedance spectroscopy (ESI) measurements are also employed to disclose electrochemical kinetics of the as-prepared $LiFePO_4$. And Nyquist plots are presented in Figure S6 (Supporting Information). The charge transfer impedance of micro/nano $LiFePO_4$, which is the main part of cathode impedance, is smaller than that of commercial $LiFePO_4$, implying the rapid ion transport kinetics as a superior cathode for high-performance LIBs.[45]

Figure 6 shows X-ray energy dispersive spectroscopy (EDS) and selected area mapping images of the $LiFePO_4$ cages with octahedral micro/nano hierarchical structure. As shown in Figure 6a, EDS image (Figure 6a) verifies that O, P and Fe elements are homogeneously distributed in the obtained materials, in which the molar ratio of P and Fe is nearly 1:1, in good accordance with XRD data in Figure 3a.

On the basis of above discussion, the high rate capacity of micro/nano hierarchical $LiFePO_4$ cages can be attributed to small size of the nanoparticle subunits which ensures short Li^+ diffusion distance. In addition, Secondary micro-sized octahedral structure prevents nanoparticle from aggregation and accommodates the volume variations, which can present high tap density and excellent cycling stability. The interstices between primary $LiFePO_4$ nanoparticles is beneficial for electrolyte penetration, accelerating the Li^+ insertion/extraction reaction. Moreover, the as-prepared micro/nano hierarchical $LiFePO_4$ cages reach up to 1.4 g cm^{-3}, which can be generally used in manufacturing real batteries for practical applications.

Conclusion

In summary, a unique monodispersed $LiFePO_4$ cages with octahedral micro/nano hierarchical structure has successfully fabricated via a controllable synthetic approach. Novel micro-sized $LiFePO_4$ cages, constructed by monocrystalline nanosized subunits, exhibit high specific surface areas of 40.631 m^2 g^{-1} with pore distribution of 31.2 nm and 53.7 nm, respectively. The large surface areas can certainly provide the sufficient interface between electrolyte and active materials, which is beneficial for enhancing electrochemical performances. When applied as a cathode material for LIBs, the $LiFePO_4$ cages exhibit high rate capability (106, 88, 76 mAh g^{-1} at rate of 5, 10 and 20 C, respectively), excellent cycling stability with capacity retention of 98% and superior tap density (1.4 g cm^{-3}). We believe that this special micro/nano structure can be extended to other lithium metal oxide composites, which would promote the development of lithium-ion batteries.

Experimental section

Materials: All chemicals or materials were used as raw material without any further purification. Ethylene Glycol (Fisher Chemical, 99.99%), Iron Nitrate ($Fe(NO_3)_3$, 99.9%, Aldrich), Sodium Dihydrogen Phosphate (NaH_2PO_4, 99.9%, Aldrich), Sodium Carbonate (Na_2CO_3, 99.9%, Aldrich), Lithium orthophosphate (Li_3PO_4, 99.9%, Aldrich) and metallic Li foil (99.9%, Aldrich).

Preparation of octahedral $Fe_3(PO_4)_2(OH)_2$ crystals: $Fe_3(PO_4)_2(OH)_2$ precursor was synthesized by a solvothermal reaction. In a typical synthesis of $Fe_3(PO_4)_2(OH)_2$ crystals, ethylene glycol (25 ml), 1M $Fe(NO_3)_3$ aqueous solution (5 ml), 1M NaH_2PO_4 aqueous solution (5 ml) and 1M Na_2CO_3 aqueous solution (1 ml), were mixed step by step under powerful stirring with intervals of 2-3 min. And then, the precursor solution was stirred for another 20 min until the mixture changes from turbidity to transparent pale yellow solution. After that the mixture solution was transferred into a Teflon-lined stainless steel autoclave with a volume of 45 ml, a thermal treatment was performed for the Teflon-liner in an electric oven at 170 ^oC for 24 hrs. After the autoclave was cooled down naturally to room temperature in the air, samples deposited at the bottom were collected and washed by centrifugation with de-ionized water (D.I. water) and pure ethanol respectively at least three cycles. Finally, the precipitates were then dried in a vacuum oven at 60 ^oC overnight to remove the residue water and ethanol for the subsequent fabrication.

Preparation of micro/nano hierarchical $LiFePO_4$ cages: Octahedral $Fe_3(PO_4)_2(OH)_2$ (100 mg) were evenly mixed with Li_3PO_4 powder in a molar ratio of 1:1 with the help of a few pure ethanol. Then appropriate amount carbon black powder was introduced into the mixture as reducing substance to form the calcinations samples. Afterwards, the samples were loaded into the tube furnace and calcined in Ar atmosphere at 700 ^oC for 200 min with a ramp of 1 ^oC/min. After cooled to room temperature, the targeted material micro/nano hierarchical structured $LiFePO_4$ was obtained.

Characterization: Field Emission Scanning Electron Microscope (FESEM, JEOL, JSM-7800F, 15 kV), high-resolution TEM (HRTEM, Philips, Tecnai, F30, 300 kV), X-ray Diffractometer with Cu Kα radiation (XRD, Bruker D8 Advance), Brunauer-Emmett-Teller surface area measurement (BET, Quantachrome Autosorb-6B surface area & Pore size analyzer), The thermogravimetric analysis (TGA, Mettler Toledo). Fourier transformation infrared spectrum (FTIR, Nicolet iS50) were employed to characterize the obtained samples. The measurement of tap density is that placing some powder in a small cylinder and tapping for 10 min by hand. The mass of the tapped powder and the measured volume are used to calculate the tap density of the product.[46]

Electrochemical measurements: A homogeneous mixture composed of the micro/nano hierarchical structured $LiFePO_4$ active material, carbon black and polyvinyl difluoride (PVDF) using 1-Methyl-2-pyrrolidinone (NMP) as a solvent with a weight ratio of 80:10:10 was prepared under vigorous magnetic stirring at least 12 hrs. Then appropriate amount of mixture were extracted and spread evenly on Al foils. Though weighed the Al foils pre-and post-treatment in a high-precision analytical balance (Sartorius, max weight 41 g, d=0.01 mg), the reading difference was the exact mass of coated samples on Al foils. The obtained pieces of Al foils covered with samples were used as working electrodes with 1 M $LiPF_6$ in 1:1 v/v ratio mixture of ethylene carbonate and diethyl carbonate. Celgard 2400 was employed as the separator film to detach the two electrodes, and pure Li foil (99.9%, Aldrich) was both served as the counter electrode and reference electrode. The cell was assembled in an argon-filled glovebox where moisture and oxygen concentrations were strictly limited to below 0.1 ppm. The galvanostatic charge-discharge tests were conducted on a LAND battery program-control test system (CT-2001A, Jinnuo electronic Co.). And cyclic voltammetry (CV) and electrochemical impedance spectrum (ESI) were collected using Autolab (model of AUT71740) in a three-electrode cell.

Acknowledgements

This work was financially supported by the Thousand Young Talents Program of the Chinese Central Government (Grant No.0220002102003), National Natural Science Foundation of China (NSFC, Grant No. 21373280， 21403019), Beijing National Laboratory for Molecular Sciences (BNLMS), the Fundamental Research Funds for the Central Universities (0301005202017) and Hundred Talents Program at Chongqing University (Grant No. 0903005203205).

Supporting Information Available: Additional materials characterization figures (SEM, HRTEM, EIS, FTIR and electrochemical testing) are available in the supporting information.

References

1. Y. Wang, Y. Wang, E. Hosono, K. Wang and H. Zhou, *Angew. Chem., Int. Ed.*, 2008, 47, 7461-7465.
2. L. Shen, H. Li, E. Uchaker, X. Zhang and G. Cao, *Nano Lett.*, 2012, 12, 5673-5678.
3. J. Yang, J. Wang, Y. Tang, D. Wang, X. Li, Y. Hu, R. Li, G. Liang, T.-K. Sham and X. Sun, *Energy Environ. Sci.*, 2013, 6, 1521-1528.
4. F. Yu, S. Ge, B. Li, G. Sun, R. Mei and L. Zheng, *Curr. Inorg. Chem.*, 2012, 2, 194-212.
5. Manthiram and Arumugam, *J. Phys. Chem. Lett.*, 2011, 2, 176-184.
6. A. K. Padhi, K. S. Nanjundaswamy and J. B. Goodenough, *J. Electrochem. Soc.*, 1997, 144, 1188-1194.
7. S. Nishimura, G. Kobayashi, K. Ohoyama, R. Kanno, M. Yashima and A. Yamada, *Nat. Mater.*, 2008, 7, 707-711.
8. Fergus and J. W., *J. Power Sources*, 2010, 195, 939-954.
9. A. Yamada, S. C. Chung and K. Hinokuma, *J. Electrochem. Soc.*, 2001, 148, A224.
10. P. P. Prosini, M. Lisi, D. Zane and M. Pasquali, *Solid State Ionics*, 2002, 148, 45-51.
11. D. Liu and G. Cao, *Energy Environ. Sci.*, 2010, 3, 1218-1237.
12. Y. S. Hu, Y. G. Guo, R. Dominko, M. Gaberscek, J. Jamnik and J. Maier, *Adv. Mater.*, 2007, 19, 1963-1966.
13. Y. Ding, Y. Jiang, F. Xu, J. Yin, H. Ren, Q. Zhuo, Z. Long and P. Zhang, *Electrochem. Commun.*, 2010, 12, 10-13.
14. F. Croce, A. D' Epifanio, J. Hassoun, A. Deptula, T. Olczac and B. Scrosati, *Electrochem. Solid-State Lett.*, 2002, 5, A47-A50.
15. S. Hamelet, M. Casas-Cabanas, L. Dupont, C. Davoisne, J. M. Tarascon and C. Masquelier, *Chem. Mater.*, 2011, 23, 32-38.
16. X. Rui, X. Zhao, Z. Lu, H. Tan, D. Sim, H. H. Hng, R. Yazami, T. M. Lim and Q. Yan, *ACS Nano*, 2013, 7, 5637-5646.
17. Y. Wang and G. Cao, *Adv. Mater.*, 2008, 20, 2251-2269.
18. X.-J. Wang, H.-Y. Chen, X. Yu, L. Wu, K.-W. Nam, J. Bai, H. Li, X. Huang and X.-Q. Yang, *Chem. Commun*, 2011, 47, 7170-7172.
19. D. W. Hoffman, R. Roy and S. Komarneni, *J. Am. Ceram. Soc.*, 1984, 67, 468-471.
20. C. Nan, J. Lu, L. Li, L. Li, Q. Peng and Y. Li, *Nano Res.*, 2013, 6, 469-477.
21. H. Shang, W. Chu, J. Cheng, F. Pan, D. Cheng, D. Xia, W. Wang and Z. Wu, *J. Mater. Chem. A*, 2013, 1, 6635.
22. J. Li, B. L. Armstrong, J. Kiggans, C. Daniel and D. L. Wood, *Langmuir*, 2012, 28, 3783-3790.
23. M. Wang, Y. Yang and Y. Zhang, *Nanoscale*, 2011, 3, 4434-4439.
24. F. Yu, J. Zhang, Y. Yang and G. Song, *J. Power Sources*, 2010, 195, 6873-6878.
25. C. Sun, S. Rajasekhara, J. B. Goodenough and F. Zhou, *J. Am. Chem. Soc.*, 2011, 133, 2132-2135.
26. X. Lou and Y. Zhang, *J. Mater. Chem.*, 2011, 21, 4156-4160.
27. H. M. Xie, R. S. Wang, J. R. Ying, L. Y. Zhang, A. F. Jalbout, H. Y. Yu, G. L. Yang, X. M. Pan and Z. M. Su, *Adv Mater.*, 2006, 18, 2609-2613.
28. Y. Zhao, L. Peng, B. Liu and G. Yu, *Nano Lett.*, 2014, 14, 2849-2853.
29. J. Su, X.-L. Wu, C.-P. Yang, J.-S. Lee, J. Kim and Y.-G. Guo, *J. Phys. Chem. C*, 2012, 116, 5019-5024.
30. S. Lan, L. Liu, R. Li, Z. Leng and S. Gan, *Ind. Eng. Chem. Res.*, 2014, 53, 3131-3139.
31. X. Qin, J. Wang, J. Xie, F. Li, L. Wen and X. Wang, *Phys. Chem. Chem. Phys.*, 2012, 14, 2669.
32. X. Qin, X. Wang, H. Xiang, J. Xie, J. Li and Y. Zhou, *J. Phys. Chem. C*, 2010, 114, 16806-16812.
33. X. Xia, Y. Zhang, D. Chao, C. Guan, Y. Zhang, L. Li, X. Ge, I. M. Bacho, J. Tu and H. J. Fan, *Nanoscale*,

2014, 6, 5008-5048.

34. J. Wang, X. Yao, X. Zhou and Z. Liu, *J. Mater. Chem.*, 2011, 21, 2544-2549.
35. Y.-F. Shi, H. Liu, G.-B. Liu and X.-W. You, *Ionics*, 2013, 19, 1503-1508.
36. C.-J. Jia, L.-D. Sun, Z.-G. Yan, L.-P. You, F. Luo, X.-D. Han, Y.-C. Pang, Z. Zhang and C.-H. Yan, *Angew. Chem., Int. Ed.*, 2005, 44, 4328-4333.
37. J. J. Chen and M. S. Whittingham, *Electrochem. Commun.*, 2006, 8, 855-858.
38. J. Chen, S. Wang and M. S. Whittingham, *J. Electrochem. Soc.*, 2007, 174, 442-448.
39. H. Fei, Z. Peng, Y. Yang, L. Li, A.-R. O. Raji, E. L. G. Samuel and J. M. Tour, *Chem. Commun.*, 2014, 50, 7117-7119.
40. G. Wang, H. Liu, J. Liu, S. Qiao, G. M. Lu, P. Munroe and H. Ahn, *Adv. Materials.*, 2010, 22, 4944-4948.
41. W. J. Zhang, *J. Electrochem. Soc.*, 2010, 157, A1040-A1046.
42. H. M. Xie, R. S. Wang, J. R. Ying, L. Y. Zhang, A. F. Jalbout, H. Y. Yu, G. L. Yang, X. M. Pan and Z. M. Su, *Adv. Materials.*, 2006, 18, 2609-2613.
43. R. Dominko, M. Bele, M. Gaberscek, M. Remskar, D. Hanzel, S. Pejovnik and J. Jamnik, *J. Electrochem. Soc.*, 2005, 152, A607-A610.
44. Y.-H. Nien, J. R. Carey and J.-S. Chen, *J. Power Sources*, 2009, 193, 822-827.
45. Z. Shi, M. Huang, K. Yang, X. Hu, B. Tan, X. Huang and Z. Deng, *J. Solid State Electrochem.*, 2012, 16, 811-818.
46. Z. Chen and J. R. Dahn, *J. Electrochem. Soc.*, 2002, 149, A1184-A1189.

Figures and Captions

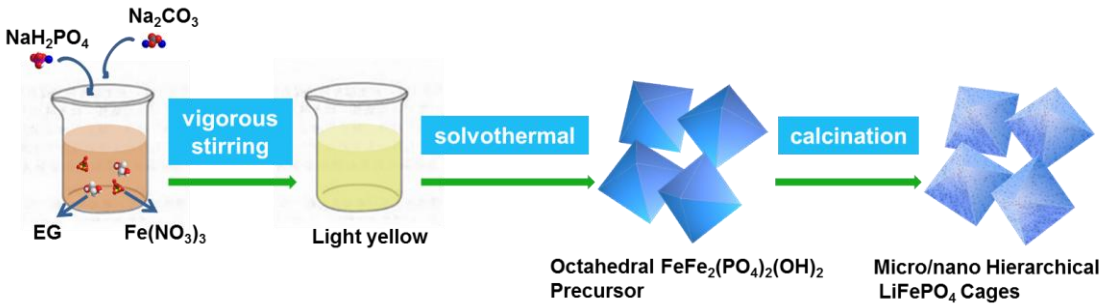

Figure 1. Schematic illustration of synthetic route to $LiFePO_4$ with octahedral micro/nano hierarchical structure.

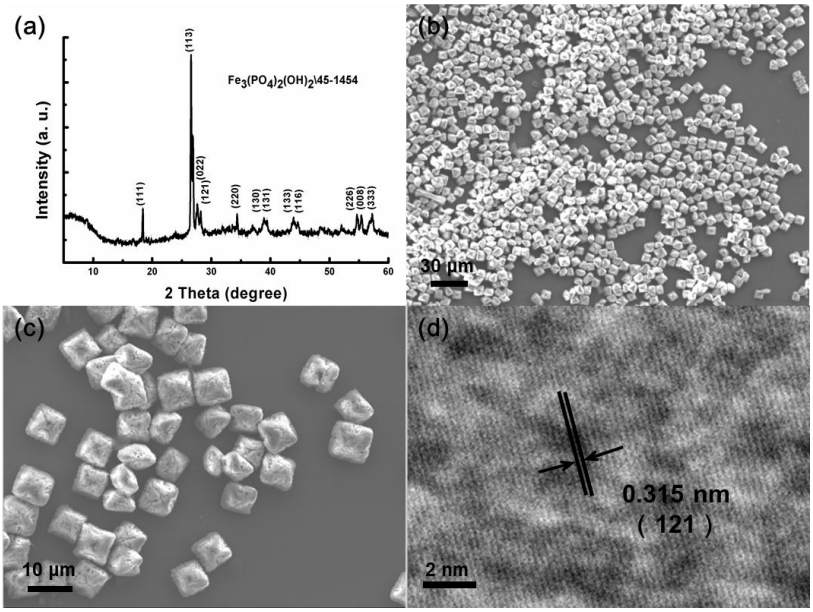

Figure 2. The phase purity and structural characterization of the octahedral $Fe_3(PO_4)_2(OH)_2$ crystals. (a) X-ray diffraction (XRD) pattern of the precursor $Fe_3(PO_4)_2(OH)_2$. (b) Scanning electron microscopy (SEM) image in large scale synthesis. (c) Enlarged SEM image of the precursor $Fe_3(PO_4)_2(OH)_2$. (d) The high-resolution TEM (HRTEM) image of well-crystallized micro-sized octahedron.

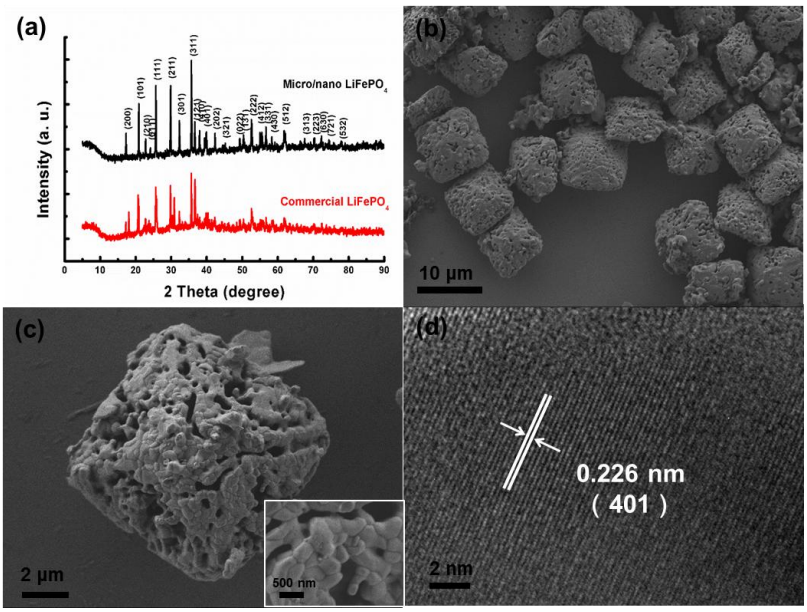

Figure 3. The phase purity and structural details of the as-prepared octahedral micro/nano hierarchical $LiFePO_4$ cages. (a) XRD patterns of micro/nano $LiFePO_4$ cages and Commercial $LiFePO_4$ powders. (b) SEM image of the as-synthesized $LiFePO_4$. (c) Representative SEM image of single octahedral micro/nano hierarchical $LiFePO_4$. Inset: intersices on the surface. (d) HRTEM image of synthesized micro/nano $LiFePO_4$ cages.

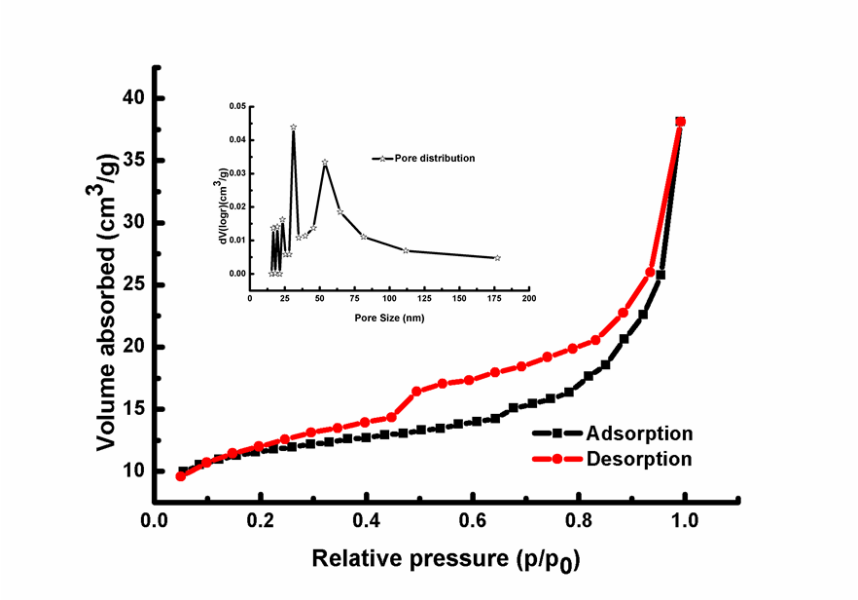

Figure 4. BET isotherm of the micro/nano $LiFePO_4$ cages to reveal the specific surface area and pore size distribution derived from the desorption branch (inset).

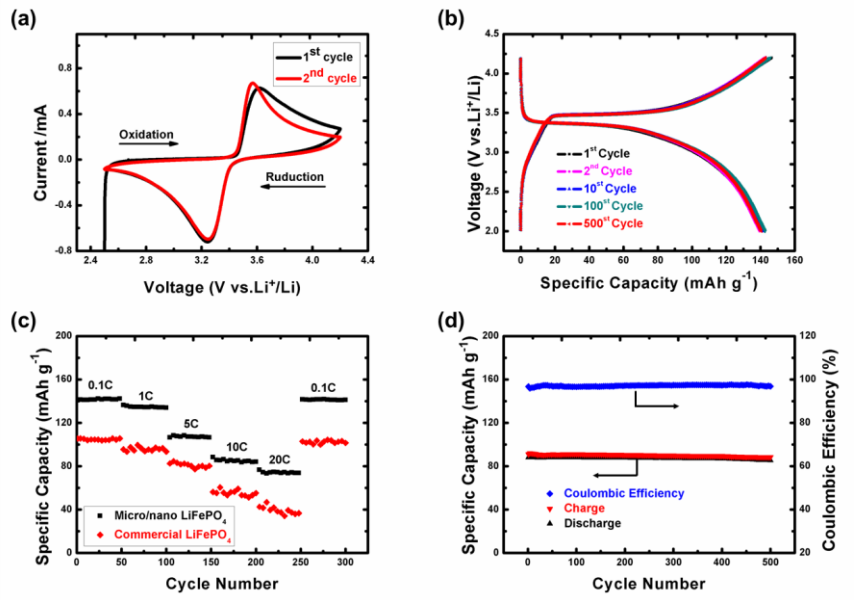

Figure 5. Electrochemical characterization of as-prepared octahedral micro/nano hierarchical $LiFePO_4$. (a) Cyclic voltammetry tests in the potential range of 2.4~4.2V (vs. Li^+/Li). (b) Charge-discharge profiles for the 500th cycles at current density of 17 mA g^{-1} (0.1 C) in the potential range of 2.0~4.2V (vs. Li^+/Li). (c) The rate performance at different current densities. (d) Cycling performances and coulombic efficiency at current density of 1700 mA g^{-1} (10 C).

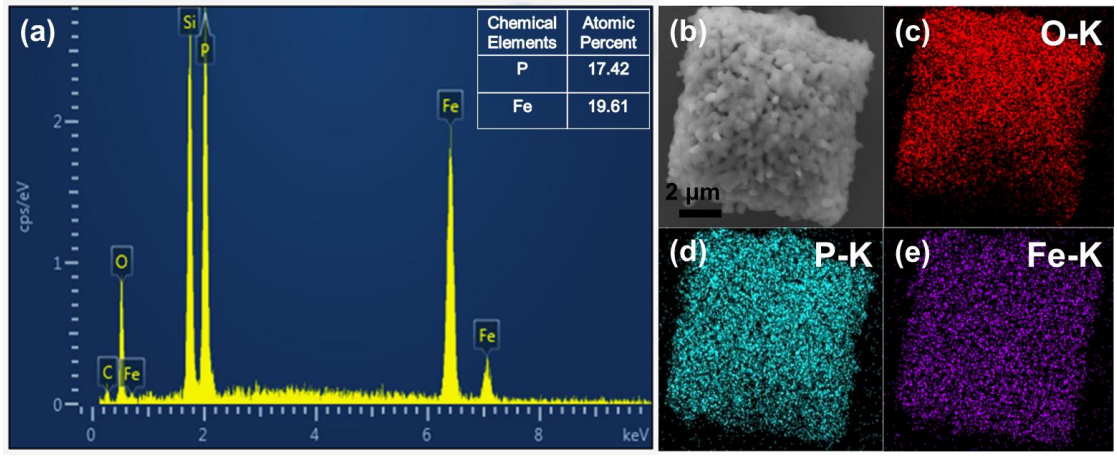

Figure 6. X-ray energy dispersive spectroscopy (EDS) and selected area mapping images of the $LiFePO_4$ cages with octahedral micro/nano hierarchical structure. EDS verifies the O, P and Fe elements in the obtained materials. The O, P and Fe elements are evenly distributed in the as-prepared materials as demonstrated in (c)-(d), respectively.